Alternative Encapsulation Material Combined with Geometric Techniques for Electric Field Mitigation within (U)WBG Packages under High Frequencies

Pujan Adhikari and Mona Ghassemi
Department of Electrical and Computer Engineering
The University of Texas at Dallas, Richardson, TX
pujan.adhikari@utdallas.edu, mona.ghassemi@utdallas.edu

2024 IEEE International Power Modulator and High Voltage Conference (IPMHVC) | 979-8-3503-4853-8/24/$31.00 ©2024 IEEE | DOI: 10.1109/IPMHVC55105.2024.11002847

***Abstract*— As power modules based on (U)WBG materials gain attention for their potential to revolutionize high-voltage, high-power density applications, their optimal performance is hindered by current insulation materials. The high electric field stress at triple points (TPs) and encapsulant's diminishing breakdown field strength at high temperatures significantly limit the application of power modules to below 200°C. Therefore, alternative encapsulation materials are essential for high-temperature applications. This paper proposes a novel solution involving replacing standard silicone gel (SG) encapsulant with high-temperature encapsulation composites created by integrating micro- and nano-sized fillers into a silicone elastomer matrix. Additionally, the ceramic structure is redesigned into a mesa configuration, featuring a trench at the base of the metal electrodes. The results from modeling and simulation of COMSOL Multiphysics demonstrate that this combined approach significantly reduces field stress at TPs. Although effective at lower frequencies, further design modifications, such as altering the metalized substrate into a protruding structure, are necessary for optimal electric field mitigation at frequencies above 10 kHz. This research addresses the critical issues of high electric field values at TPs and the limited temperature tolerance of current encapsulation materials, which are challenges exacerbated under high-frequency square pulse operation. By resolving these issues, this work represents a valuable advancement in utilizing high-voltage, high-power density (U)WBG power modules at demanding frequency environments.**

Keywords—(U)WBG power module packaging, triple points, high frequency, high voltage, alternative encapsulation material, geometric techniques, high power density

I. Introduction

The operation of power modules at high voltage and power density relies on the use of wide bandgap (WBG) materials such as silicon carbide (SiC) and gallium nitride (GaN), alongside ultra-wide bandgap ((U)WBG) materials like diamond, and aluminum nitride (AlN). These materials provide significantly higher blocking voltages than traditional silicon-based devices, and they support higher slew rates (dv/dt) and frequency voltage pulses [1]. However, it is crucial to recognize that high slew rates and frequencies are critical factors that profoundly influence the performance and reliability of insulation systems [2, 3]. Ceramic substrate (e.g., AlN, Al_2O_3) and encapsulation material (e.g., SG, EP) are the insulation materials within the power modules. The substrate, which electrically insulates the components within the system while dissipating heat, is soldered into the metal electrodes, and the whole structure is encapsulated by encapsulation material that shields the system from dirt, and severe weather conditions. The high electric field and consequently partial discharge (PD) issue in (U)WBG power module stems from the formation of TPs at the junction of the metallization layer, substrate, and encapsulant and the presence of metalized protrusions during manufacturing [4-7].

Even though techniques like nonlinear field-dependent conductivity (FDC) layers [8-13], nonlinear field-dependent permittivity (FDP) materials, and geometric redesigning have been considered to mitigate the electric field at TPs, this still doesn't resolve the thermal issues associated with the conventional encapsulants, thereby limiting the performance of power modules to temperatures <200°C [2, 4]. Encapsulation materials prepared by incorporating fillers like AlN and SiC into original silicone matrices have been proposed for use in high-temperature scenarios and have successfully demonstrated better PD performance [14, 15]. However, their implementation for electric field reduction has rarely been conducted, and even if it has been conducted, it hasn't been performed for high-frequency square waveforms. It has been validated that high frequency increases the electric field at TPs, causes space charge accumulation, increases electrical tree lengths, and worsens PD activity [16, 17]. Therefore, this paper combines a micro-SiC and nano-AlN-filled silicone elastomer encapsulant with two geometric techniques, i.e., mesa structure and protruding substrate, to realize optimal electric field mitigation under high-frequency scenarios. It is observed that even though electric fields rise with frequency, this strategy effectively reduces the electric fields of the insulation system within limits.

II. Conventional Structure and Its Simulation Results

Simulations are performed in COMSOL Multiphysics to replicate the practical conditions of (U)WBG power module packages to estimate the electric field and mitigate it at the TPs if it is higher than the limit. IEC 61287-1 states that power modules must meet the one-minute insulation test requirement with an AC voltage of $V_{rms} = (2U_b/\sqrt{2}+1)$ kV, where U_b is the module's blocking voltage. For our module with 25 kV blocking voltage, V_{max}= 51.41 kV. Thus, AlN is used as the substrate with a thickness of 51.41/25 =2.06 mm and a length of 4.074 mm. The electrical conductivity and relative permittivity of AlN substrate and SG encapsulant are 10^{-11} S/m and 10^{-13} S/m, and 9 and 2.86, respectively. To replicate the practical conditions, protrusions having 12 µm height and 37 µm length are considered for both metallization edges atop the substrate. Since electric field values are higher around TPs and gradually reduce when moving away from TPs, a uniform

This work was partially funded by the U.S. National Science Foundation (NSF) under Award 2306093.

meshing strategy doesn't work. That's why three meshing zones were defined as having different numbers of elements: zone 1, zone 2, and zone 3 having maximum element sizes of 2 µm, 40 µm, and 400 µm, respectively. Based on IEC 61287-1 guideline, for a SiC power module with a blocking voltage of 25 kV, the voltage applied to the high voltage electrode is a square waveform of 1.1 × 25 = 27.5 kV at 60 Hz frequency, while the other electrode is grounded. Fig. 1 depicts conventional structures' electric field distribution plots, showing an undesirably high electric field concentrated around TPs and protrusions. The electric field is measured with measuring lines at a distance of 15 µm from the sharp edges and TPs. The electric field intensity along lines L1 (HV SG), L2 (LV SG), L3 (HV AlN), and L4 (LV AlN) are 85.8, 26.93, 78.2, and 23.28 kV/mm, respectively. These high values of electric field centered around TPs should be mitigated if power modules are to be worked under high voltage and power density.

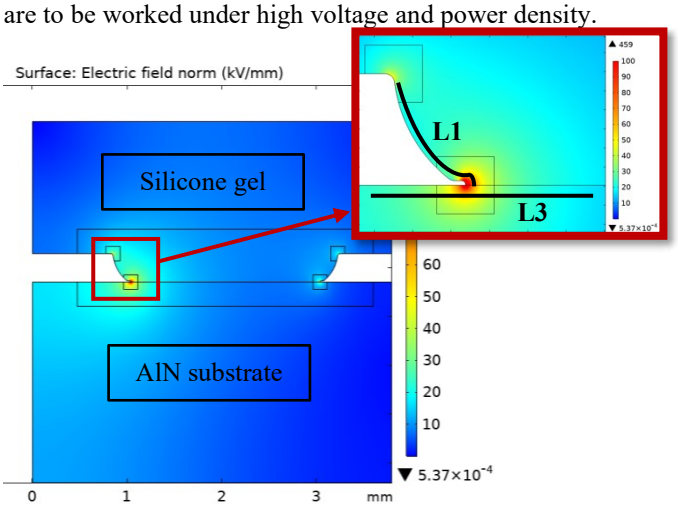

Fig 1. Electric field distribution plot showing high electric field at TPs.

III. Mesa Structure Combined with Alternative Encapsulation Material

A. Micro- and Nano-particle Filled Encapsulation Material

One strategy to reduce the electric field at TPs might be the replacement of SG with an alternative encapsulation material prepared by incorporating micro- and nanoparticles in a silicone matrix. It has been validated in several experiments that incorporating these filler particles in original silicone and epoxy matrixes helps suppress the PD issues and improve the breakdown strength. However, the use of these composites for electric field reduction has rarely been performed. For example, using nanocomposite, Chen et.al. [15] observed the reduction of the electric field at TP from 36.9 kV/mm to 7.4 kV/mm. However, this simulation was done for MV SiC power modules under DC voltage, which might not simulate the practical operation of (U)WBG power modules at much higher and square wave voltages of very high frequencies. Therefore, in this study, the composite which showed the best dielectric and thermal characteristics is chosen for FEM simulation. The encapsulation material (S20N3) is prepared by incorporating 20 wt.% micro SiC and 3 wt.% nano AlN particles in silicone elastomer matrix. The principle of how these materials achieve electric field reduction is based on nonlinear conductivity characteristics. The nonlinear conductivity is related to the electric field based on equation (1):

$$\sigma(E) = \sigma_0(1 + (E/E_b)^{\alpha-1}) \quad (1)$$

For our encapsulation material, the low field conductivity (σ_0), the switching field (E_b), and the nonlinearity coefficient (α) are takem as 3.83×10^{-14} S/m, 1.75 kV/mm, and 6.12.

B. Mesa Structure

The primary cause of the significantly uneven electric field and subsequent premature insulation failure in power modules stems from the TPs. Eliminating the sharp metal edges at the junction of metallization layers, substrate, and encapsulation material could potentially resolve this issue. To achieve this, a mesa structure is implemented by reducing the height of the substrate, thereby creating a trench with specific dimensions between the HV and ground electrodes [18]. In our simulation, we consider a mesa structure with a height of 300 µm and a width of 2 mm between the electrodes. The trench is designed with a rounded base to eliminate sharp edges that could induce high electric fields, as depicted in Fig. 2.

C. Simulation Results

Fig. 2 illustrates the electric field distribution when the micro-SiC and nano-AlN-filled encapsulation material is combined with a mesa structure, and a square wave voltage of 27.5 kV is applied at 60 Hz. It can be seen from the plot that when SG is replaced by the alternative encapsulant and mesa structure is introduced, the electric field at both substrate and encapsulant regions is significantly reduced. The electric field values along the four lines L1, L2, L3, and L4 are 35.28, 25.72. 25.68, and 9.7 kV/mm, respectively. The 59%, 5%, 67%, and 58% reduction in the electric field along lines L1, L2, L3, and L4 are achieved due to replacing SG with an alternative encapsulant and introducing the mesa structure. Even though these reductions are significant compared to the conventional structure and the electric field around the AlN substrate remains reasonable (typical dielectric strength of 20-30 kV/mm), the electric field around the encapsulant region surpasses that of a typical encapsulation material which is 15-20 kV/mm.

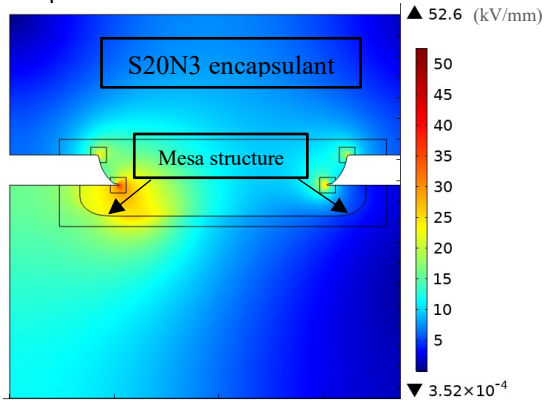

Fig 2. Electric field distribution plot for combined mesa structure and alternative encapsulation material (α=6.12 & E_b=1.75 kV/mm)

The reason why the electric field of the substrate is reduced more than the encapsulant can be explained by the fact that when mesa structure is introduced, the substrate area moves away from the protrusions that still exist in the encapsulant region and contributes to a high electric field. This effect becomes more prominent when we apply voltage pulses with higher frequencies, which can be observed later in section V, Fig. 4. As

seen from the figure when the frequency increases from 60 Hz to 100 kHz, the electric field intensity along line L1 increases by 151%. Therefore, in the next section, we analyze whether eliminating the protrusions helps mitigate the high field issue.

IV. Protruding Substrate Combined with Mesa Structure and Alternative Encapsulation Material

In this section, we investigate the impact of introducing a rounded structure to the metalized substrate, forming a protruding substrate, as illustrated in Fig. 3, on reducing the electric field in the encapsulation region.

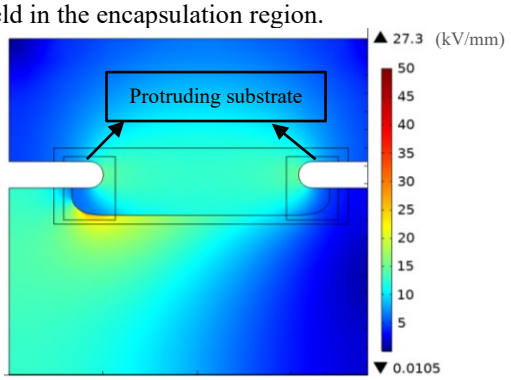

Fig 3. Electric field distribution plot for combined protruding substrate, mesa structure, and alternative encapsulation material (α=8.12 & E_b=0.75 kV/mm)

Initially, simulations are conducted using power frequency square voltage, where it is observed that the protruding substrate decreases the electric field along lines L1 and L2 to 29.98 and 19.55 kV/mm, respectively. Although this represents a reduction of 17.7% and 24% compared to scenarios without the protruding substrate, the electric field values remain elevated. This persistent high electric field around the encapsulant, despite the presence of alternative encapsulant and protruding substrate, can be elucidated as follows: the alternative encapsulant contributes to reducing the electric field by attaining a nonlinearity characteristic beyond the switching field, thereby forming conductive paths that impede the accumulation of charge particles at TPs. Consequently, the efficacy of the encapsulant hinges on these two parameters. It has been stated that a higher nonlinearity coefficient and a lower switching field lead to the material achieving nonlinearity sooner and at a faster rate. These parameters can be adjusted by modifying the matrix's size and concentration of filler particles. However, it is noteworthy that drastically altering these parameters could be impractical, as an increase in filler concentration may introduce additional issues such as heightened viscosity, interfacial defects, and the formation of cavities. Fig. 3 illustrates the electric field distribution plot for the protruding substrate combined with a mesa structure and alternative encapsulant with α= 8.12 and E_b= 0.75 kV/mm. As the diagram shows, this approach significantly diminishes the electric field around the substrate and encapsulant region. The electric field values along lines L1, L2, L3, and L4 measure 14.91, 14.84, 25.04, and 14.52 kV/mm, respectively. This translates to 50.3% and 24.1% reduction around encapsulant regions of HV and grounded electrodes, respectively. Another noteworthy achievement is the uniformity in the electric field across the insulation system around both the HV and grounded metallization layers, as evidenced by the plot.

After establishing the strategy's effectiveness for power frequency square voltages, it's crucial to investigate its efficacy at higher frequencies. It is evident from research articles [4, 15] that higher frequency exacerbates insulation failure by inducing higher electric field stresses and more PD pulses, thereby reducing the partial discharge inception voltage (PDIV). To observe this influence, the electric field values for the combination of protruding substrate, mesa structure, and alternative encapsulants at various frequencies were observed. Encapsulants with different α and E_b parameters are considered to examine their influence on electric field mitigation.

Table I presents the values of electric field intensity for alternative encapsulants combined with the two geometric techniques at frequencies from 60 Hz to 100 kHz. As observed from the table, the increment in the electric field around line L1 is significant for encapsulant A with α=6.12 & E_b=1.75 kV/mm when the frequency is increased to 100 kHz, rising by 71.7% compared to 60 Hz. However, the electric field values for the alternative encapsulant B with α=8.12 & E_b=0.75 kV/mm remain within the dielectric strength of both the insulation materials at all the frequencies. The increment in the electric field around line L1 is only 20.6% when the frequency is increased from 60 Hz to 100 kHz, which is almost a three times reduction compared to encapsulant A. This robust reduction in electric field stress validates the strategy's effectiveness in mitigating the high electric field issue of (U)WBG power modules at high frequencies.

TABLE I. ELECTRIC FIELD FOR ALTERNATIVE ENCAPSULANTS WITH PROTRUDING SUBSTRATE AND MESA STRUCTURE

Optimization Strategies	Electric Field (kV/mm) Along Measurement Lines at Various Frequencies				
	Frequency	*Line L1*	*Line L2*	*Line L3*	*Line L4*
Alternative Encapsulant A with α=6.12 & E_b=1.75 kV/mm	60 Hz	29.98	19.55	23.63	9.09
	1 kHz	38.83	19.34	25.44	7.52
	10 kHz	48.69	18.99	25.91	7.32
	50 kHz	51.35	18.97	25.95	7.3
	100 kHz	51.46	18.96	25.96	7.3
Alternative Encapsulant B with α=8.12 & E_b=0.75 kV/mm	60 Hz	14.84	14.84	25.04	14.52
	1 kHz	14.91	14.87	24.68	14.54
	10 kHz	15.02	14.99	23.76	14.71
	50 kHz	16.63	15.55	24.03	15.16
	100 kHz	17.9	15.65	24.29	15.27

V. Comparison of Electric Field Mitigation with and without Protruding Substrate at Various Frequencies

From the simulation results obtained in sections III and IV, it's evident that introducing a protruding substrate leads to a significant reduction in electric field stress. In this section, we analyze and compare the electric field values along lines L1 and L2 for structures with and without a protruding substrate, considering both encapsulation materials. Given that the introduction of the mesa structure already contributes to the reduction in the substrate's electric field within limits, it is unnecessary to compare the electric field along lines L3 and L4. As depicted in Fig. 4, when the metalized substrate is redesigned into a protruding substrate, the electric field is decreased along both lines for alternative encapsulant A. Moreover, this reduction is further amplified at higher frequencies. However, despite these improvements, the electric field values remain relatively high. Consequently, encapsulant B was deemed a more favorable choice due to its superior performance in reducing electric field stress. As observed in Fig. 5, even in the

absence of a protruding substrate, the electric field values are notably lower for encapsulant B compared to the previous case, attributed to its superior nonlinearity feature. Nevertheless, at higher frequencies, the electric field of the encapsulant surpasses acceptable limits and therefore, we achieve more favorable outcomes by implementing a protruding structure. Another study on this topic can be found in [19].

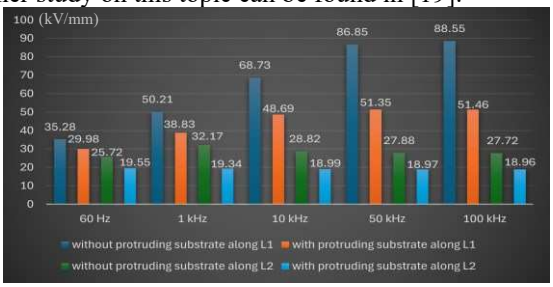

Fig 4. Electric field values (kV/mm) at various frequencies for alternative encapsulation material (α=6.12 & E_b=1.75 kV/mm)

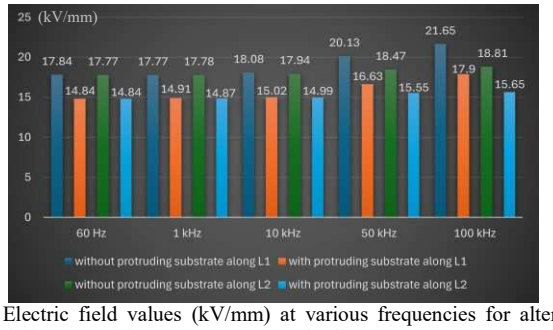

Fig 5. Electric field values (kV/mm) at various frequencies for alternative encapsulation material (α=8.12 & E_b=0.75 kV/mm).

VI. Conclusion

This study presents an innovative approach to mitigate high electric field stresses in (U)WBG power modules under high-frequency operations by combining advanced encapsulation materials with geometric design modifications. Integrating micro- and nano-sized fillers into a silicone elastomer matrix and implementing a mesa structure significantly reduced electric field intensity. Even though the maximum electric field along line L1 was reduced to 35.28 kV/mm at power frequency square voltage, the electric field dramatically increased to 88.55 kV/mm at 100 kHz, suggesting that this strategy won't be enough to achieve electric field mitigation at high frequencies. When the material properties of the encapsulant were changed to have better nonlinear conductivity characteristics, it was seen that the electric field along that line was reduced to 21.65 kV/mm, a 75.5% decrement. However, the electric field can further be reduced around the encapsulant region if the mesa structure implementing alternative encapsulation material is combined with a protruding substrate. This structure helps eliminate the protrusions at the sharp metal edges, reducing the maximum electric field to 14.84 kV/mm at 60 Hz and 17.9 kV/mm at 100 kHz. Furthermore, the electric field distribution plot shows that the electric field stress is uniformly distributed in both the substrate and encapsulant regions, thereby ensuring better operation of (U)WBG power modules under demanding conditions of high frequencies.

References

[1] P. Adhikari and M. Ghassemi, "A comprehensive review of mitigation strategies to address insulation challenges within high-voltage, high-power-density (U)WBG power module packages," *IEEE Trans. Dielectr. Electr. Insul.*, vol. 31, no. 5, pp. 2676-2700, Oct. 2024.

[2] P. Adhikari, and M. Ghassemi, "Navigating Strategies to Mitigate Insulation Issues within High Power Density (U)WBG Power Module Packages: A Comprehensive Review Emphasizing Alternative Encapsulation Materials," *IEEE Trans. Ind. Appl.*, Early Access.

[3] M. Ghassemi, "Accelerated insulation aging due to fast, repetitive voltages: A review identifying challenges and future research needs," *IEEE Trans. Dielectr. Electr. Insul.*, vol. 26, no. 5, pp. 1558–1568, Oct. 2019.

[4] B. Zhang, M. Ghassemi, and Y. Zhang, "Insulation materials and systems for power electronics modules: A review identifying challenges and future research needs," *IEEE Trans. Dielectr. Electr. Insul.*, vol. 28, no. 1, pp. 290–302, Feb. 2021.

[5] M. M. Tousi and M. Ghassemi, "Combined geometrical techniques and applying nonlinear field dependent conductivity layers to address the high electric field stress issue in high voltage high-density wide bandgap power modules," *IEEE Trans. Dielectr. Electr. Insul.*, vol. 27, no. 1, pp. 305–313, Feb. 2020.

[6] P. Adhikari and M. Ghassemi, "A review of insulation challenges and mitigation strategies in (U)WBG power modules packaging," *IEEE Texas Power Energy Conf. (TPEC)*, 2024, pp.1-6.

[7] P. Adhikari, E. Arafat, S. P. Kalakonda, and M. Ghassemi, "Investigating partial discharge characteristics in silicone gel for (U)WBG power modules under negative DC voltage: a comparative study of optical and electrical detection methods," *IEEE Conf. Electr. Insul. Dielectr. Phenomenon (CEIDP)*, 2024, pp. 1-4.

[8] M. M. Tousi and M. Ghassemi, "Electric field control by nonlinear field dependent conductivity dielectrics characterization for high voltage power module packaging," *IEEE Int. Workshop Integr. Power Packag. (IWIPP)*, 2019, pp. 54-58.

[9] M. M. Tousi and M. Ghassemi, "Electrical insulation packaging for a 20 kV high density wide bandgap power module," *IEEE Energy Convers. Congr. Expo. (ECCE)*, 2019, pp. 4162-4166.

[10] M. Mesgarpour Tousi and M. Ghassemi, "Effects of frequency and temperature on electric field mitigation method via protruding substrate combined with applying nonlinear FDC layer in wide bandgap power modules," *Energies*, vol. 13, no. 8, p. 2022, 2020.

[11] M. M. Tousi and M. Ghassemi, "The effect of type of voltage (sinusoidal and square waveform) and the frequency on the performance of nonlinear field-dependent conductivity coatings for electric field control in power electronic modules," *IEEE Conf. Electr. Insul. Dielectr. Phenomena (CEIDP)*, 2019, pp. 552-555.

[12] M. M. Tousi and M. Ghassemi, "Nonlinear field dependent conductivity materials for electric field control within next-generation wide bandgap power electronics modules," *IEEE Electr. Insul. Conf. (EIC)*, 2019, pp. 63-66.

[13] M. M. Tousi and M. Ghassemi, "Nonlinear resistive electric field grading in high-voltage, high-power wide bandgap power module packaging," *IEEE Energy Convers. Congr. & Expo. (ECCE)*, 2019, pp. 7124-7129.

[14] X. Chen *et al.* "Potential of epoxy nanocomposites for packaging materials of high voltage power modules: A validation using experiments and simulation," *IEEE Trans. Dielectr. Electr. Insul.*, vol. 28, no. 6, pp. 2161–2169, Dec. 2021.

[15] X. Chen *et al.* "Enhancement of electrical properties by including nano-aluminum nitride to micro-silicon carbide/silicone elastomer composites for potential power module packaging applications," *J. Mater. Sci. Mater. Electron.*, vol. 33, no. 23, pp. 18768–18785, Aug. 2022.

[16] Y. Zhang *et al.*, "Electrical tree evolution of BN sheet/epoxy resin composites at high voltage frequencies," *IEEE Trans. Dielectr. Electr. Insul.*, vol. 29, no. 5, pp. 1991–1999, Oct. 2022.

[17] C. Dai, Y. Tanaka, H. Miyake, K. Sato, X. Chen, and A. Paramane, "Space charge dynamics in epoxy based composites under dc and square pulse wave of different polarities and frequencies," *IEEE Trans. Dielectr. Electr. Insul.*, vol. 28, no. 6, pp. 1980–1987, Dec. 2021.

[18] H. Hourdequin *et al.*, "Metallized ceramic substrate with mesa structure for voltage ramp-up of power modules," *Eur. Phys. J. Appl. Phys.*, vol. 87, no. 2, Art. no. 2, Aug. 2019.

[19] P. Adhikari and M. Ghassemi, "Characterizing nonlinear field dependent conductivity layers to mitigate electric field within (U)WBG power modules under high frequency, high slew rate square voltage pulses," *IEEE Texas Power Energy Conf. (TPEC)*, 2024, pp. 1-6.